KTH Fysik

In-beam Study of ^{106}Te and ^{107}Te Using Recoil-Decay Tagging

BAHARAK HADINIA

Licentiate Thesis in Physics
Stockholm, Sweden, 2006

TRITA-FYS 2006:46
ISSN 0280-316X
ISRN KTH/FYS/–06:46–SE
ISBN 91-7178-407-1

KTH
SE-100 44 Stockholm
SWEDEN

Akademisk avhandling som med tillstånd av Kungl Tekniska högskolan framlägges till offentlig granskning för avläggande av Teknologie licentiatexamen 060616 i Sal FB55, Albanova university centrum, Roslagstullsbacken 21, Stockholm.

Tryck: Universitetssevice US AB

Abstract

Atomic nuclei are complex many-body systems and exhibit an interplay between single-particle and collective degrees of freedom. In order to describe and predict the "behavior" of nucleons inside the nuclei a variety of theoretical models have been created, each applicable to their own domain of nuclear phenomena. Experimental information is needed in order to test and improve the various theoretical models with the ultimate goal of creating unified theory of nuclear structure. In-beam γ-ray spectroscopy is one way of probing the inner structure of nuclei and it is the subject of this thesis, which describes the first identification of excited states in the extremely neutron deficient nuclei ^{106}Te and ^{107}Te. The experiments were performed at the Accelerator Laboratory of the University of Jyväskylä, Finland, using the recoil-decay tagging technique. Prompt γ rays emitted following fusion evaporation reactions were detected by the Jurogam detector array and the selection of the γ rays of interest was based on the recoil identification provided by the RITU gas-filled recoil separator and the GREAT focal plane spectrometer. The production cross sections were estimated to be 25nb and $1\mu b$ for ^{106}Te and ^{107}Te, respectively. In case of the nucleus ^{106}Te, several γ rays have been observed. A vibrational-like yrast band has been suggested. For ^{107}Te a number of γ rays have been assigned and a tentative partial level scheme has been suggested. The experimental data have been compared to shell model calculations.

List of Publications

This thesis is based on the two first papers in the list.

1-**First identification of γ-ray transitions in ^{107}Te**. B.Hadinia, B.Cederwall, K.Lagergren, J.Blomqvist, T.Bäck, S.Eeckhaudt, T. Grahn, P.Greenlees, A.Johnson, D.T.Joss, R.Julin, S.Juutinen, H.Kettunen, M.Leino, A.-P.Leppänen, R.J.Liotta, P.Nieminen M.Nyman, J.Pakarinen, E.S.Paul, P.Rahkila, C.Scholey, J.Uusitalo, R.Wadsworth, D.R.Wiseman,
Phys. Rev. C70, 064314 (2004).

2-**First identification of excited states in ^{106}Te and evidence for isoscalar-enhanced vibrational collectivity**. B.Hadinia, B.Cederwall, K.Andgren, J.Blomqvist, I.Darby, S.Eeckhaudt, E.Ganioğlu, P.Greenlees, E.Ideguchi, P.M.Jones, D.T.Joss, R.Julin, S.Ketelhut, M.Leino, E.S.Paul, M.Petri, P.Rahkila, M.Sandzelius, C.Scholey, J.Uusitalo, R.wadsworth, R.Wyss
Phys. Rev. C72, 041303(R) (2005).

3- First identification of excited states in the ^{93}Pd. D.Sohler, K.Lagergren, J.Blomqvist, B.Cederwall, A.Johnson, B.Hadinia, L.Milechina, J.Timar, G.de Angelis, P.Bednarczyk, D.Curien, A.Gadea, J.Nyberg,
Eur. Phys. J. A19, 169-172 (2004).

4- Recoil-decay tagging of γ-rays in the extremely neutron-deficient nucleus ^{162}Os. D.T.Joss, K.Lagergren, D.E.Appelbe, C.J.Barton, J.Simpson, B.Cederwall, B.Hadinia, R.Wyss, S.Eeckhaudt, T.Grahn, T.Greenless, P.M.Jons, R.Julin, S.Suutinen, H.Kettunen, M.Leino, A.-P.Leppänen, P.Nieminen, J.Pakarinen, P.Rahkila,C.Scholey, J.Uusitalo, R.D.Page, E.S.Paul, D.R.Wiseman,
Phys. Rev. C70, 017302 (2004).

5- Probing structural changes in the very neutron-deficient Os isotopes with recoil-decay tagging. D.T.Joss, N.Amzal, D.E.Appelbe, T.Back, C.J.Barton, M.A.Bentley,

B.Cederwall, J.F.C.Cocks, D.M.Cullen, S.Eeckhaudt, T.Grahn, P.T.Greenlees, B.Hadinia, K.Helariutta, P.M.Jones, R.Julin, S.Juutinen, H.Kankaanpaa, A.Keenan, H.Kettunen, S.L.King, P.Kuusiniemi, K.Lagergren, M.Leino, A.P.Leppänen, M.Muikku, P.Nieminen, R.D.Page, J.Pakarinen, E.S.Paul, P.Rahkila, C.Scholey, A.Savelius, J.Simpson, M.J.Taylor, J.Uusitalo, S.J.Williams, D.D.Warner, D.R.Wiseman, R.Wyss.
J.Phys. G31, (2005) S1593.

6- Yrast structures in the light Pt isotopes $^{169-173}$Pt. D.T.Joss, J.Simpson, D.E.Appelbe, K.Lagergren, C.J.Barton, B.Cederwall, S.Eeckhaudt, T.Grahn, P.M.Jones, R.Julin, S.Juutinen, B.Hadinia, H.Kettunen, M.Leino, A.-P.Leppänen, P.Nieminen, R.D.Page, J.Pakarinen, E.S.Paul, J.Perkowski, P.Rahkila, M.A.Riley, C.Scholey, J.Uusitalo, K.Van de Vel, D.D.Warner, D.R.Wiseman
J. Phys. G31, (2005) S1715.

7- In-beam and decay spectroscopy of very neutron deficient iridium nuclei. C.Scholey, M.Sandzelius, S.Eeckhaudt, T.Grahn, P.T.Greenlees, P.Jones, R.Julin, S.Juutinen, M.Leino, A.-P.Leppänen, P.Nieminen, M.Nyman, J.Perkowski, J.Pakarinen, P.Rahkila, P.M.Rahkila, J.Uusitalo, K.Van de Vel, B.Cederwall, B.Hadinia, K.Lagergren, D.T.Joss, D.E.Appelbe, C.J.Barton, J.Simpson, D.D.Warner, I.G.Darby, R.D.Page, E.S.Paul, D.Wiseman
J. Phys. G31, (2005) S1719.

Contents

Chapter 1

Introduction to Nuclear Structure

One of the major aims in nuclear physics is to gain a better understanding of the internal structure of atomic nuclei. The atomic nucleus is a quantum system with a size of about 10^{-14} m to 10^{-15} m. It contains protons and neutrons which interact strongly with each other, and is an excellent environment for studying a many-body quantum system with a finite (non-statistical) number of particles. The nuclear shell model was one of the first models that was created to describe the structure of nuclei. It has proved to be very successful to describe nuclei near closed shells. Lately an extension of the model using Monte carlo techniques has allowed one to analyse microscopically even heavy nuclei with many protons and neutrons outside closed shells. Today there are a number of models which have their specific domains where they can explain a limited number of experimentally observed phenomena, but no universal nuclear model exists. A goal of experimental nuclear structure physics is to provide stringent tests of nuclear models so that theory can advance towards a more fundamental understanding of nuclei. This chapter provides an introduction to a few basic nuclear models suitable for the region of nuclei under study in this thesis.

1.1 The Nuclear Shell Model

Maria Goeppert Mayer and a group including Otto Haxel, Hans Jensen and Hans Suess simultaneously and independently came to equivalent conclusions about the nuclear shell structure in 1949 [1]. If residual shell model interactions are neglected each individual nucleon moves independently in an average field produced by the other nucleons. The Schrödinger equation can then be written [2]:

$$H_0\psi(r) = [\sum_i^A h_i]\psi(r) = \sum_i^A [T_i + V(r_i)]\psi(r) = E\psi(r) \tag{1.1}$$

where ψ can be the product of the eigenfunctions ϕ_n of the single-particle Schrödinger equation

$$h_i\phi_{n_i}(r_i) = \epsilon_{n_i}\phi_{n_i}(r_i). \tag{1.2}$$

Solving the Schrödinger equation gives wave functions (eigenfunctions) and the energy eigenvalues (eigenstates) of possible nuclear states that are available for a system of nucleons.

In the shell model the eigenstates are obtained by filling the single-particle energy levels while obeying the Pauli principle. Thus, the wave function must be antisymmetric with respect to the exchange of coordinates of any pair of nucleons. This can not be fulfilled by a simple product of single particle wave functions. An antisymmetric wave function was given by John Slater and is known as the Slater determinant, which is expressed as follows:

$$\psi = \frac{1}{\sqrt{N!}} \begin{vmatrix} \phi_{n_1}(r_1) & \phi_{n_1}(r_2) & \cdots \\ \phi_{n_2}(r_1) & \phi_{n_2}(r_2) & \cdots \\ \vdots & \vdots & \ddots \end{vmatrix} \tag{1.3}$$

where N is the number of nucleons. From here follows that if one tries to put two nucleons in the same quantum state the resulting wave function ψ is zero.

The main challenge when using a shell model description is the choice of the one-body potential V(r). Since the nucleons generate the potential, it should have a radial dependence corresponding to the nuclear density. One simple form that can be used is the Wood-Saxon potential which for spherical nuclei is written as:

$$V(r) = -V_0[1 + exp(\frac{r - R_0}{a})]^{-1}, \tag{1.4}$$

where V_0 is the depth of the potential well which varies with N and Z. $R_0 = r_0 A^{1/3}$ is the nuclear radius (where r_0=1.25 fm) and the parameter a is the skin thickness over which the potential changes from 0.9 V_0 to 0.1 V_0 that also depends upon the number of nucleons and usually is around $\approx 0.5 - 0.7$ fm. Solving the Schrödinger equation with this simple potential yields the magic numbers 2, 8, and 20. By adding the strong nuclear spin-orbit interaction,

$$\begin{aligned} V_{so} &= f(r) l \cdot s \\ f(r) &= -V_{ls} \frac{\partial V(r)}{\partial r} \end{aligned} \tag{1.5}$$

to the potential, the remaining magic numbers (28, 50, 82, 126, ...) can be reproduced. In (1.5) V(r) is the potential and V_{ls} is the strength constant [3].

However, in order to have a better result one must consider residual interactions between nucleons. The N-nucleon Hamiltonian limited to two-body interactions can be written :

$$H = \sum_i T_i + \sum_{i \neq j} V_{ij} = \sum_i (T_i + V(r)) + (\sum_{i \neq j} V_{ij} - \sum_i V(r)) = H_0 + H_{res} \quad (1.6)$$

Here H_0 is the single-particle energy and H_{res} is the sum of the two-body matrix elements due to the residual interactions. It follows from (1.6), that one can simplify the H_{res} calculation by choosing a nucleus with closed shells as a reference core and only study the configurations with a few particles and holes relative to it. From studies of light nuclei using "ab initio" calculations it has recently been found that also three-body interactions play an important role in nuclei. However such interactions can not easily be applied to a large number of nucleons due to the quickly increasing calculational complexity.

This thesis contains a shell model calculation for ^{106}Te performed by Jan Blomqvist [4]. ^{106}Te has two protons and four neutrons outside the closed $N = Z = 50$ shells. In the calculation the $d_{5/2}$ and $g_{7/2}$ subshells were chosen as basis for the valance protons and neutrons. From the data on the light Sn isotopes it is known that the $d_{5/2}$ and $g_{7/2}$ subshells are close in energy and separated from the higher $s_{1/2}$, $d_{3/2}$, and $h_{11/2}$ subshells by a substantial gap. Therefore the truncation of the basis to the $d_{5/2}$ and $g_{7/2}$ subshells is reasonable. From light Sn nuclei the single-particle energies for both protons and neutrons are chosen to be $\varepsilon(d_{5/2}) = 0$ and $\varepsilon(g_{7/2}) = 120$ keV. In this basis there are a total of 102 two-body interaction matrix elements ($< j_1 j_2, JM|V_{12}|j_3 j_4, JM >$). This number reduced to 43 with the assumption of charge independence.

1.2 Deformation

The shape of a nucleus can be described by an expansion in spherical harmonics. The nuclear radius $R(\theta, \phi)$ can be expressed as:

$$R(\theta, \phi) = R_0 \left(1 + \sum_{\lambda=1}^{\infty} \sum_{\mu=-\lambda}^{\lambda} \alpha_{\lambda\mu} Y_{\lambda\mu}(\theta, \phi) \right) \quad (1.7)$$

For a spherical nucleus $R(\theta, \phi)$ reduces to R_0. The term $\lambda = 1$ is called the dipole term. The effect of this term is a shift in the center of mass. If the origin of the coordinate system is at the center of mass the coefficient $\alpha_{1\mu}$ is zero. The quadrupole deformation, $\lambda = 2$, is described by five coefficients. The quadrupole-deformed shape of a nucleus is often more simply described by two parameters β_2 and γ, defined as follows [5]:

$$\alpha_{20} = \beta_2 \cos\gamma; \alpha_{2\pm1} = 0; \alpha_{2\pm2} = \frac{1}{\sqrt{2}} \beta_2 \sin\gamma \quad (1.8)$$

The range of these parameters is $\beta_2 \geq 0$ and $-120^\circ < \gamma < +60^\circ$ which is illustrated in Fig. 1.1.

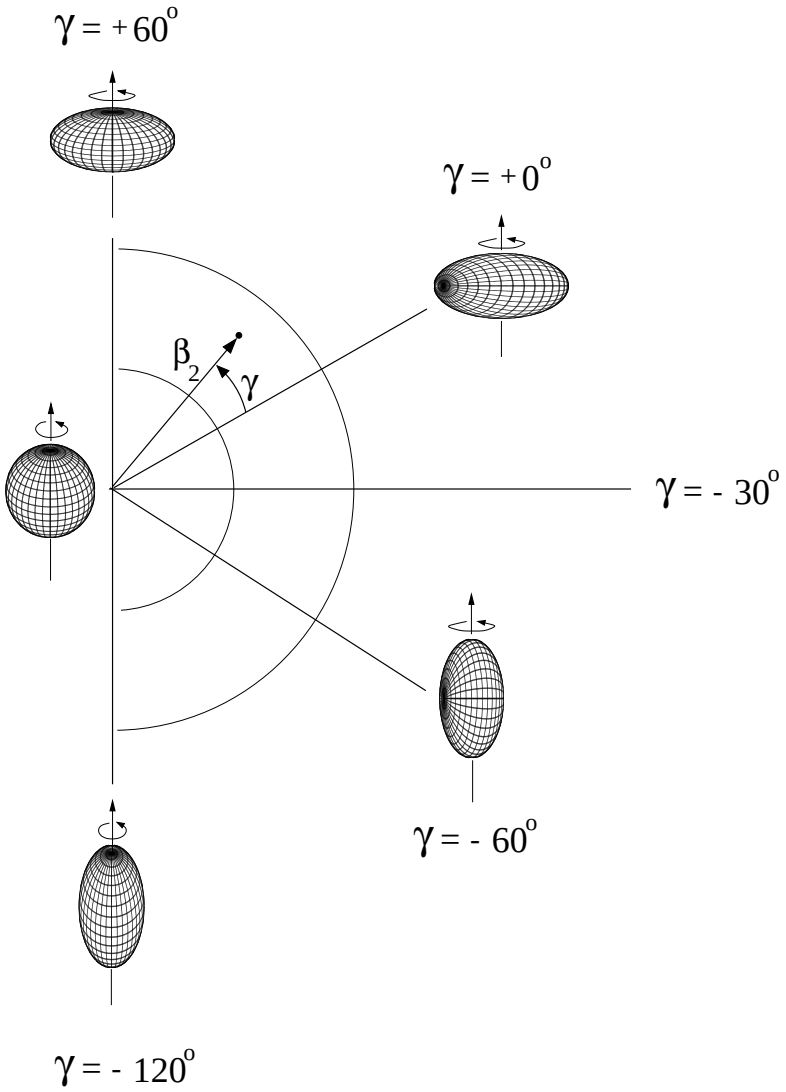

Figure 1.1: Schematic diagram of the shape parameters in rotating quadrupole-deformed nuclei. The $\gamma = 60°$ axis corresponds to the non-collective oblate (rotation around the symmetry axis) shape, γ =0° to collective prolate (rotation perpendicular to the symmetry axis) shape, γ =-60° to collective oblate and γ =120° to non-collective prolate shape. The figure is taken from reference [6].

1.3 The Liquid-Drop Model

The liquid-drop model is a model that describes the nucleus as a drop of incompressible nuclear fluid. This fluid made of nucleons is kept together by the strong nuclear force. The model is able to account for "macroscopic" properties of the nuclei that can not yet be described accurately by pure quantum models like the shell model. The liquid drop model was first proposed by George Gamow in 1928. The Weizsäcker binding energy is an empirically refined form of the liquid drop model and is given by:

$$B = E_V + E_S^0 + E_c^0 + E_{sym} + E_{pair}$$
$$B = a_{vol}A - a_{sur}A^{2/3} - a_c Z(Z-1)A^{-1/3} - a_{sym}\frac{(A-2Z)^2}{A} + \delta \qquad (1.9)$$

where the five terms give the volume binding energy, surface binding energy, Coulomb repulsion energy, symmetry energy, and the pair energy [7, 8]. The Coulomb repulsion and the surface binding energy are shape dependent; therefore, in order to apply the liquid drop model to deformed nuclei some modification is needed. Using equation (1.7), the Coulomb repulsion and surface binding energies are up to second order given by [9]

$$E_S = E_S^0(1 + \frac{1}{8\pi}\sum_{\mu,\lambda}(\lambda-1)(\lambda+2)|\alpha_{\lambda\mu}|^2)$$
$$E_c = E_c^0(1 - \frac{5}{4\pi}\sum_{\mu,\lambda}\frac{\lambda-1}{2\lambda+1}|\alpha_{\lambda\mu}|^2). \qquad (1.10)$$

The energy difference between a deformed and a spherical shape is :

$$E_S + E_c - E_S^0 - E_c^0 = E_S^0\left(\frac{2}{5}(1 - \frac{E_c^0}{2E_S^0})a_2^2 - \frac{4}{105}\sqrt{\frac{5}{4\pi}}(1 + \frac{E_c^0}{E_S^0})a_2^3 + \dots\right) \qquad (1.11)$$

where $a_2 = (5/4\pi)^{1/2}\beta_2$. These energy differences can be used to find minima and maxima in the deformation energy. Neglecting third and higher order terms in equation (1.11) the minimum is at $\beta_2 = 0$ which corresponds to a spherical shape. If $\frac{E_c^0}{2E_S^0} < 1$ the curvature is positive, thus it is stable against small deformation. For $\frac{E_c^0}{2E_S^0} > 1$ the repulsive Coulomb force is larger than the surface energy, and the nucleus will be unstable against deformation and fission. In this model the stable shape is always found to be spherical, and it is therefore unable to explain the properties of deformed nuclei. However, the liquid drop model has been successfully combined with the deformed shell model using a method developed by Strutinsky [10, 11]. Adding quantal "shell effects" also nuclei with stable deformations, which are abundant for nucleon numbers far from the closed spherical shell gaps, can be predicted.

1.4 Collective Motion

Collective excitations are considered to be nuclear transitions that involve many of the nucleons [12]. Nuclei having collective properties are usually those with many valence nucleons, that is, those with proton or neutron numbers that are far from filled shells. For such nuclei the performance and interpretation of the shell model calculations are complicated. In contrast, the collective model allows calculations of spins, parities, and transition probabilities that are in good agreement with the measured properties of the collective nuclei. Rotation and vibration are examples of collective degrees of freedom and have been described in detail by e.g. Bohr and Mottelson [13, 14].

1.5 Vibrations

A simple model for nuclear vibrations is based on small-amplitude vibrations of a liquid drop. For a quadrupole distortion ($\lambda = 2$) (see Fig.1.2), the Hamiltonian is given by

$$H = T + V = \frac{1}{2}B\sum_{\mu}|\dot{\alpha}_{2\mu}|^2 + \frac{1}{2}C\sum_{\mu}|\alpha_{2\mu}|^2, \tag{1.12}$$

The coefficients B and C play the same role as the mass and the restoring force, respectively, in classical mechanics. Each $\alpha_{2\mu}$ oscillates with a frequency $\omega = \sqrt{C/B}$ and the vibration energy is $\hbar\omega$. It is possible to define operators that create and destroy vibrational quanta, phonons. The harmonic spectrum of energy levels obtained by solving the Schrödinger equation with the Hamiltonian from equation (1.12) is shown in Fig.1.2. The same approach can be used for higher multipole distortions. More details can be found in standard nuclear physics textbooks, e.g. [3, 9]. The ratio of 2 between the excitation energies of the 4^+ and 2^+ states is a signature of a harmonic vibrator structure. However, it is not expected that nuclei should behave as ideal harmonic vibrators. Various effects, e.g. static deformations can lead to an harmonicities and the breaking of the level degeneracies seen in Fig.1.2. In this thesis evidence for vibrational structures in the tellurium isotopes is discussed in terms of the systematics of such energy ratios [4]. A complementary test would be to study transition rates. These show a characteristic pattern for vibrational excitations, being proportional to the number of vibrational phonons building up each excited state. The one-phonon rule also states that transitions can only occur that remove one vibrational quantum at a time. However, the nuclei studied in this work are highly unstable and situated far from the β-stability line. They can only be studied in reactions where they are populated with extremely small cross sections. The techniques used for measuring transition rates require large statistics and can unfortunately not be easily applied to these extremely neutron deficient tellurium isotopes.

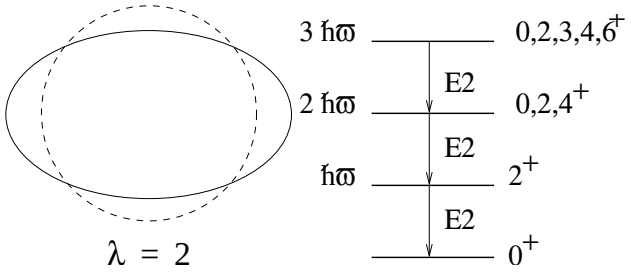

Figure 1.2: To the left a schematic quadrupole vibration is shown. To the right, a corresponding harmonic spectrum of energy levels is illustrated with the possible spin-parities given on the right.

1.6 TRS plots

A certain type of theoretical calculations can predict the energy of a nucleus as a function of the deformation parameters, the rotational frequency, the parity of the single-particle configuration and an additional quantum number called signature. The model combines the shell model, extended to deformed nuclei, with the liquid drop model. Such calculations are called Total Routhian Surface (TRS) calculations [15]. A TRS plot shows the minimum energy for a given configuration energy of the nucleus as a function of β_2 and γ. This plot can be used to find out the model predictions for the most stable deformations. This thesis includes TRS calculations for the nucleus ^{106}Te [4]. As an example, Fig. 1.3 displays a TRS plot for ^{106}Te. The nucleus is considered to be "soft" with respect to a shape deformation when a range of possible shapes are allowed within a relatively small energy range. This feature is called γ-softness if the possible range is varying in γ values. The shape of the nucleus is sensitive to the configuration of the last particles outside closed shells and therefore prolate and oblate shapes can coexist at the same excitation energy. For β-softness the possible range of the nuclear state is varying in the β value which make the nuclei become susceptible to β vibration and centrifugal stretching in rotational bands. In Fig. 1.3 it can be seen that the nucleus ^{106}Te is predicted by TRS calculations to be relatively soft with respect to shape changes near a spherical shape. In particular, it is most easily deformed along the prolate axis and might therefore be susceptible to small-amplitude β-vibrations.

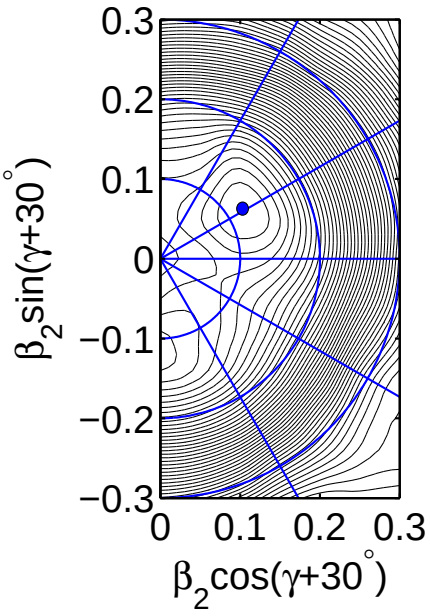

Figure 1.3: Total routhian surface plot for ^{106}Te. The energy spacing between contour lines is 200 keV. The minimum (indicated by the solid circle) point is located at a prolate shape with $\beta \approx 0.12$.

Chapter 2

Experimental Overview

2.1 Experimental Motivation

The neutron-deficient nuclei in the mass $A \approx 100$ region, close to the proton dripline, are predicted to exhibit a variety of phenomena. Of particular interest is the doubly magic nucleus ^{100}Sn, the heaviest $N = Z$ nucleus believed to be bound. Although the level structure of ^{100}Sn is not accessible with the technology available today, important pieces of information can be obtained by studying excited states of its neighbours. Information on the structure of these nuclei will provide stringent tests of the nuclear shell model in this exotic region of the nuclear chart. For instance, residual neutron-proton correlations are believed to be particularly important since neutrons and protons near the Fermi level occupy identical orbitals. Such correlations have been a topic of great interest in recent years. Theoretical models predict that isoscalar ($T = 0$) neutron-proton pair correlations may become important close to the N=Z line, leading to new nuclear structure effects. Another possible effect of enhanced neutron-proton correlation near N=Z is an increase in collectivity since the neutrons and protons may form a more strongly correlated system facilitating coherent collective motion.

A strong astrophysical motivation to study the structures of ^{106,107}Te has emerged in recent years. The rp process is a rapid proton capture process followed by slower β^+ decay. Via the rp process a number of proton rich isotopes are believed to be created. It is predicted by Schatz *et al.* [16] that there is natural termination of the rp process at nuclei with $Z \leq 52$. This is due to (γ, α) reactions, leading to a closed Sn-Sb-Te cycle, e.g, ^{105}Sn(p,γ) $\rightarrow^{106}$Sb(p,γ) $\rightarrow^{107}$Te(γ, α) $\rightarrow^{103}$Sn. The rp process extends beyond Sn if its corresponding A+1 Sb isotone is proton bound and the (γ, p) photodisintegration cross section is small. The Sn-Sb-Te cycle occurs in this model prediction since the $^{106-108}$Te nuclei are not α bound and the (γ, α) photodisintegration cross section is large. The Sn-Sb-Te cycle includes (γ, α) reactions on ^{106}Te and ^{107}Te and is therefore sensitive to the level structures of these nuclei. Experimental information on the low-lying energy spectra of the extremely

neutron deficient tellurium isotopes ^{106,107}Te, which are candidates for end point elements in the rp process, is of importance for testing the predictions and the resulting production rates for proton-rich elements up to A=107.

2.2 Introduction to Recoil-Decay Tagging Technique

Recoil-decay tagging (RDT) is an elegant and powerful technique which can be used for in-beam studies of excited states in heavy and proton rich nuclei [17, 18]. In order to apply this technique, it must be possible to identify the reaction products by detecting their emitted particles. In an RDT experiment using a fusion-evaporation reaction the compound nuclei are produced in highly excited states. They initially deexcite quickly (on a time scale of $\approx 10^{-18}s$) by particle evaporation. Depending on the number of evaporated particles and their properties, different nuclei will be produced. They deexcite toward their ground states by emitting γ rays. Such "prompt" γ-ray emission usually happens within a time range of the order of picoseconds up to a few nanoseconds. Taking into account the typical recoil velocity in fusion-evaporation reactions, this means that the γ rays are emitted close to the reaction point.

The experiments performed in this work utilise the existence of an "island" of α-emitting isotopes close to the proton dripline at $A \geq 100$. The high selectivity of the RDT technique hence enables γ-ray spectroscopic studies of nuclei which would be inaccessible with conventional in-beam methods. The emitted γ rays were detected by germanium detectors which were distributed around the target chamber. A thin target foil is chosen in order to avoid stopping the reaction products inside the target. The reaction products are separated from scattered beam ions by the gas-filled recoil separator RITU (Recoil Ion Transport Unit) [19, 20]. The separation is based on the difference in rigidity between the recoils and scattered beam when passing through a magnetic field as described in section (2.5). A carbon charge reset foil of 40 μg/cm^2 thickness was placed immediately downstream of the target in order to equilibrate the charge distributions of the recoiling fusion products and the beam particles. The recoiling fusion products pass through RITU and are implanted into a double-sided silicon strip detector (DSSD) of the GREAT spectrometer at the focal plane of RITU. The unstable implanted recoils decay inside the DSSDs with time distributions that depend on their half lives. Signals from all detectors are recorded with a "time stamp", and spatial and temporal correlations between the recoil implants and their corresponding decays are found off-line. By performing both energy and time correlations, each given α or proton decay energy "uniquely" identifies its mother nucleus. In the present work we have relied on earlier measurements of the α-decay energies of ^{106,107}Te. However since nuclear masses increase $\approx$ parabolically as a function of N-Z along an isobaric chain the α-decay energies increase with increasing neutron deficiency. New exotic isotopes are therefore generally characterised by larger α or proton decay energies and also by much lower production cross sections than previously known isotopes.

Since all events are available with time information from a 100 MHz clock it is possible to correlate the prompt γ rays corresponding to each individual identified reaction product with the ground-state decays occurring up to seconds or even minutes later. In the set-up for an RDT experiment some additional equipment such as a multi-wire proportional avalanche counter (MWPAC), Si PIN photodiodes, Planar and Clover Ge detectors are placed near the RITU focal plane. Their applications will be explained in detail in the following sections. Fig. 2.1 shows a schematic picture of the experimental set-up.

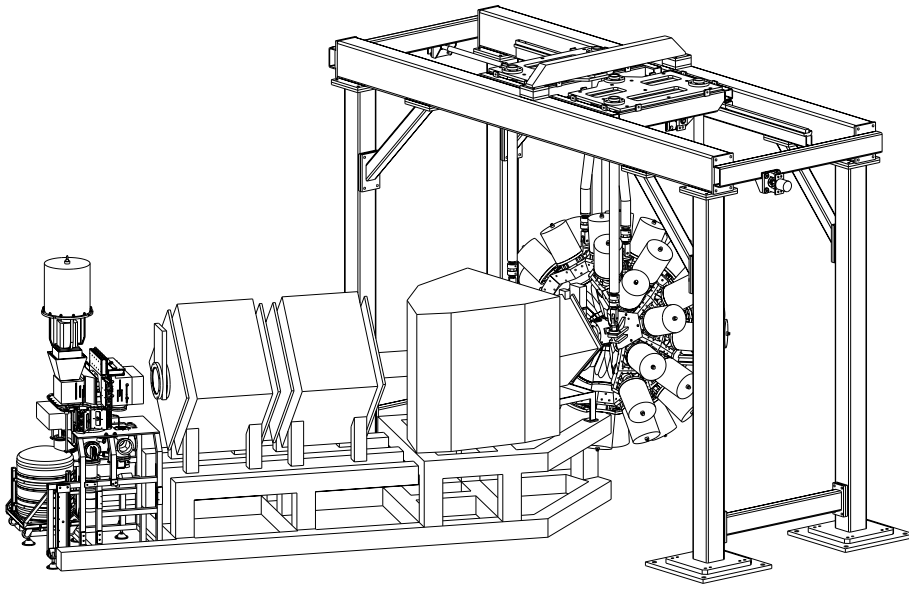

Figure 2.1: A schematic picture of the experimental setup consisting of the germanium detector array (Jurogam), the recoil separator (RITU), and the GREAT system, which is placed at the focal plane of RITU. The figure is taken from reference [21].

2.3 Population and Decay of High-Spin States

Several conditions must be fulfilled when a compound nucleus is formed. First, the beam particles must have enough energy to overcome the Coulomb barrier of the beam-target system. The height of the Coulomb barrier in the center of mass frame

is approximately given by:

$$E_{CB}(MeV) = \frac{1.44 Z_1 Z_2}{1.16(A_1^{1/3} + A_2^{1/3})} \tag{2.1}$$

where Z_1, A_1, Z_2 and A_2 are the atomic numbers and masses of the beam and target nuclei, respectively. Second, the transferred angular momentum should not be too large, in order to avoid overly rapid rotation which causes the centrifugal repulsion to overcome the short-range attractive nuclear force, leading to fission. A compound nucleus has an excitation energy that depends on the Q value of the corresponding reaction, on the beam energy and on the masses of the beam and target nuclei. The typical excitation energy for compound nuclei is 40 MeV and the maximum angular momentum is typically around $50\hbar$. The compound nucleus starts the deexcitation by evaporating light particles. Each particle takes away a significant part of the excitation energy from the system, but only a small amount of angular momentum. Fig. 2.2 displays schematically the stages from the creation of a compound nucleus to the ground state.

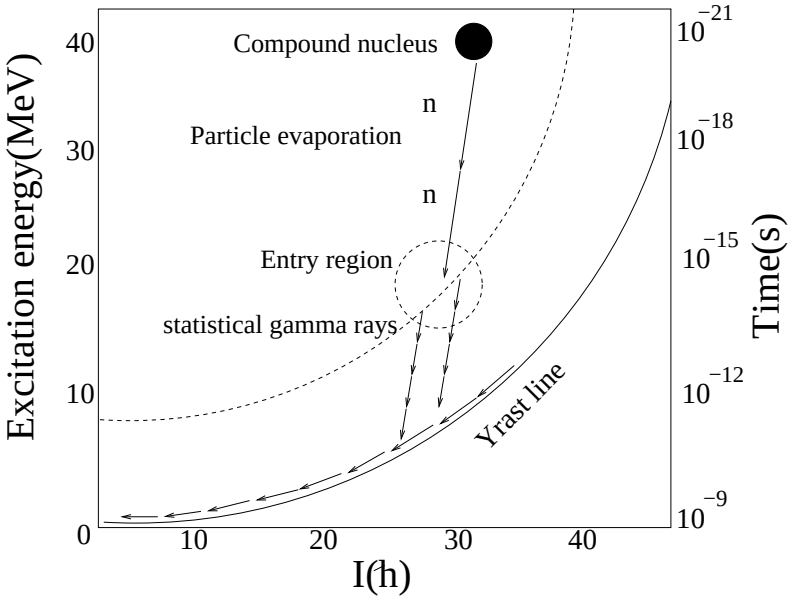

Figure 2.2: Schematic illustration of the decay of a compound nucleus. In the shown example two neutrons were evaporated. The dashed line corresponds to the particle evaporation threshold. The figure is adapted from reference [22].

2.4 Detection of γ-ray Radiation with JUROGAM

The K130 cyclotron of the Jyväskylä University Accelerator Laboratory was used to accelerate the ^{52}Cr and ^{54}Fe ions utilised in the experiment. Target foils made of highly enriched ^{58}Ni and ^{54}Fe material were bombarded by these ion beams to produce ^{107}Te and ^{106}Te via evaporation of neutrons. The prompt γ rays emitted in the decay from highly excited states towards the ground state were detected using the germanium detector array Jurogam [23] placed at the target position. Jurogam consists of 43 Compton-suppressed Eurogam Phase I and GASP-type HPGe detectors. These are distributed over six rings around the target chamber with five detectors at 158° relative to the beam direction, ten at 134°, ten at 108°, five at 94°, five at 86° and eight at 72°. The total photo-peak efficiency of the Jurogam array is about 4.2% at 1.3 MeV. In Fig. 2.3 a photo of the Jurogam array is shown.

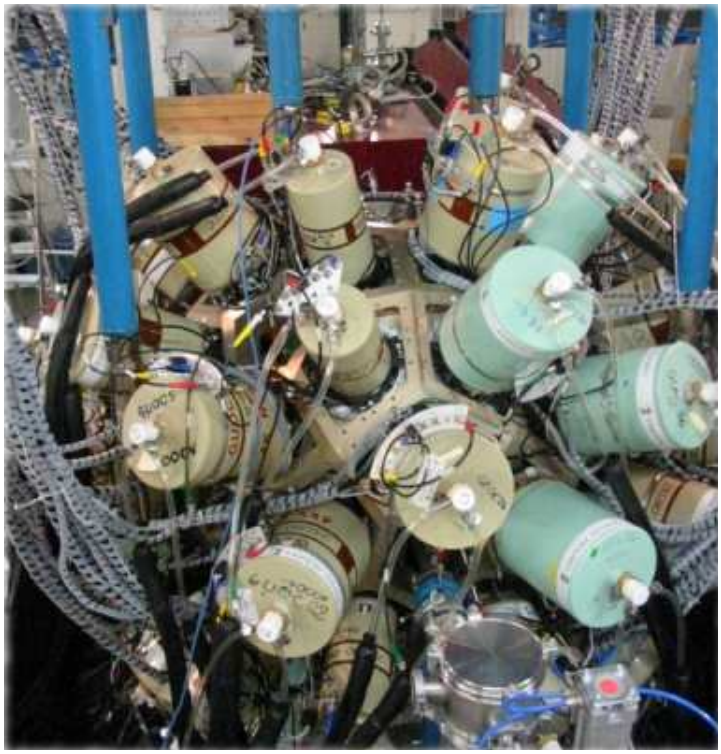

Figure 2.3: A photo of the Jurogam array.

2.5 The Gas-Filled Recoil Separator

The gas-filled recoil separator RITU [19, 20] consists of four strong magnets in a QDQQ configuration, where Q is a quadrupole magnet and D is a dipole magnet. Its vacuum chamber is filled with helium gas at pressure that is typically around 1 mbar. The gas filled region is separated from the high vacuum region upstream the target chamber by means of a powerful "differential" pumping system. The gas inside the RITU chamber decreases the angular range over which the charged ions are distributed by means of charge equilibration. This increases the transmission of the recoils. A disadvantage is that there is no distinction between different masses and different charge states. Fig. 2.4 compares schematically vacuum and gas-filled recoil separators. In Fig. 2.5 is displayed a schematic picture of RITU in the central position of the experimental set-up.

The beam-recoil separation is based on the deflection of the moving charged particles by the magnetic field of strength B. This can be discussed in terms of rigidity ($R = Br$) where r is the radius of the particle trajectory in the magnetic field. It can be formulated as follows [24]:

$$R = \frac{m_0 v}{e q_{av}} \approx \frac{m_0 v}{\frac{v}{v_0} e Z^{1/3}} = \frac{0.0227A}{Z^{1/3}}[Tm] \tag{2.2}$$

where v_0 (the Bohr velocity) is c/137, m_0 is the rest mass, q_{av} is the average charge state, and Z is the atomic number of the recoil nucleus. There is usually large difference in rigidity between beam particles and fusion products since the latter generally have significantly lower velocities. However, the heavier the beam particles are, the smaller is this difference. For studies of heavy neutron deficient nuclei the beam-target mass asymmetry is normally quite large and a good separation is easily achieved. However, the nuclei studies in this work can only be reached in near-symmetric fusion-evaporation reactions leading to difficulties in beam recoil separation.

2.6 The GREAT Spectrometer

The GREAT (Gamma Recoil Electron Alpha Tagging) spectrometer is placed in conjunction with the recoil separator at the focal plan of RITU. GREAT consists of several distinct components: a multi-wire proportional avalanche counter (MWPAC), two double-sided silicon strip detectors (DSSD), a double-sided planar germanium strip detector, a high-efficiency segmented germanium Clover-type detector and an array of silicon PIN photo-diode detectors.

The MWPAC is placed immediately before the DSSDs, and the recoils pass through it before being implanted into the DSSDs. The MWPAC signal acts as a start time for the time-of-flight measurements between the MWPAC and the DSSDs and also contains information on the deposited energy. This information enables us to distinguish the reaction products from scattered beam particles and from the

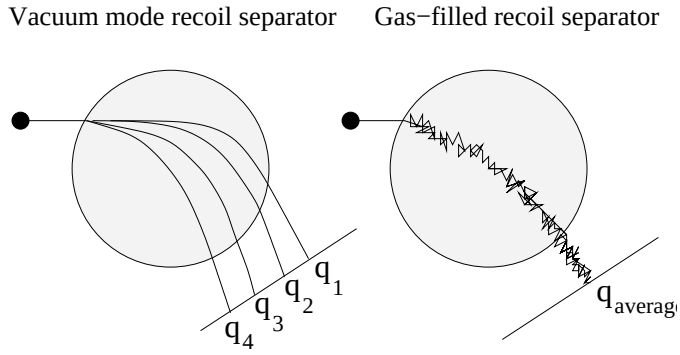

Figure 2.4: Schematic Illustration of two different designs of recoil separators. The shaded part displays an area with a magnetic field pointing perpendicular out of the page. The ions travel from left to right.

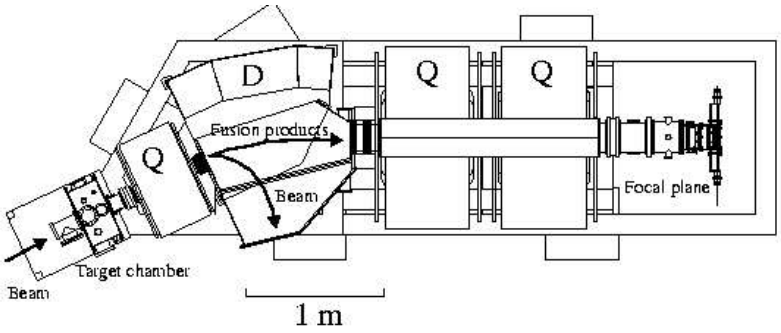

Figure 2.5: Schematic picture of the Recoil Ion Transport Unit (RITU). The quadrupole and dipole magnets are marked in the picture. The dark area indicates the gas-filled region. The figure is taken from reference [25]

decay alpha particles or protons. Fig. 2.6 shows a two-dimensional histogram with the time-of-flight information on the x-axis and the deposited energy on the y-axis. It is possible to select events that correspond to fusion-evaporation products as shown in Fig. 2.6. Thus it is possible to avoid background arising from implantation of scattered beam in the DSSDs. The PIN detectors can be used to measure conversion electron energies and to detect alpha particles which have escaped from the DSSDs. The germanium planar detector can be used to detect β decay electrons and delayed low-energy γ rays originating from decay of isomeric states or following α or proton decay of the residual nuclei. The clover germanium detector can be used to detect such γ rays with energies up to several MeV.

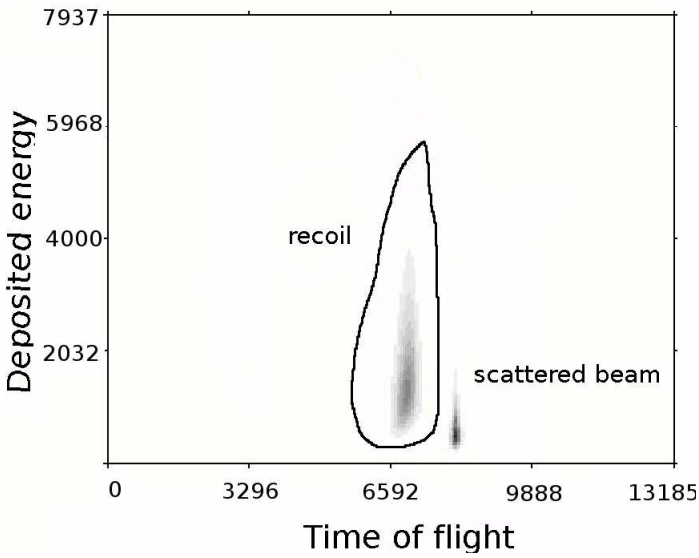

Figure 2.6: Histogram of the deposited energy in the MWPAC versus time of flight between the MWPAC and the DSSDs. The gate used to select the recoil distribution is indicated. Scattered beam particles appear to the lower right of this gate. Time increases from right to left.

2.7 The Total Data Readout (TDR) System

In a RDT experiment the time delay between the detection of γ rays by germanium detectors at the target position and the charged particle decay by the Si detectors at the focal plane plays an important role. This time delay is equal to or larger than the flight time of the fusion-evaporation productions from the target to the focal plane. The total data readout (TDR) [26] system, which is a trigger-less data acquisition system, reads out all channels independently with no time losses. The

collected data are associated with a time stamp generated by a 100 MHz clock. This gives an accuracy of 10 ns. The events can be then reconstructed in software. The GRAIN software package [27] and the Tscan software code [28] were used in order to analyze data on-line and off-line.

2.8 Data Analysis

The first step in the data analysis is to perform accurate calibrations of energy and time spectra. The energy spectra from different detectors are aligned by translating the ADC (Analog to Digital Converter) channel numbers to energies using known sources. For linear amplifiers the energy of the detected γ rays or charged particles can usually be expressed as a nearly linear polynomial function of the ADC channel number. If there is a more severe nonlinearity in the amplifier or the ADC a different function must be found, but the linear part still normally dominates over higher-order terms. The ADCs used for the Jurogam germanium detectors have significant deviations from linearity for small signal amplitudes.

The 43 detectors of the Jurogam array are as previously mentioned placed at different angles with respect to the beam direction. Since the γ rays are emitted from recoiling nuclei moving at high velocity, they are Doppler shifted. The Doppler shift depends on the angle between the detector and the beam direction (recoil direction) and on the velocity of the recoiling fusion product. The detected γ-ray energy must be corrected using the formula

$$E_\gamma = E_{\gamma D}\frac{1-\beta cos\theta}{\sqrt{1-\beta^2}} \tag{2.3}$$

Here $E_{\gamma D}$ is the measured energy of a γ transition, E_γ is its energy value in the rest frame, $\beta = v/c$, and θ is the angle at which the detector is placed, measured relative to the beam direction. The Doppler effects also leads to uncertainties in the measured γ-ray energies. One contribution to this "Doppler broadening" comes from the opening angles of the Ge detectors. By differentiating equation (2.3) with respect to θ it is seen that this effect is approximately proportional to $\beta sin\theta$, i.e. it is worst at $\theta = 90°$. Another contribution comes from the straggling of the recoils in the target, leading to a spread in the recoil directions.

The detected γ rays are assigned to specific reaction channels by associating them with the corresponding recoil nuclei. In a RDT experiment the identification of the recoil is, as mentioned in section (2.2), done via identification of its decay particle. It has been done by applying time and position correlation between an implanted recoil and its particle decay. This is drawn schematically in Fig. 2.7. The spacial and temporal correlation is done by searching for α characteristic decay energy in each individual pixel of the DSSDs considering a proper search time after each recoil implantation. If the half life of the nucleus of interest is known the search time is usually taken to be around three half lives. However, care must be

taken to avoid random background events if the recoil rate is large relative to the inverse half life.

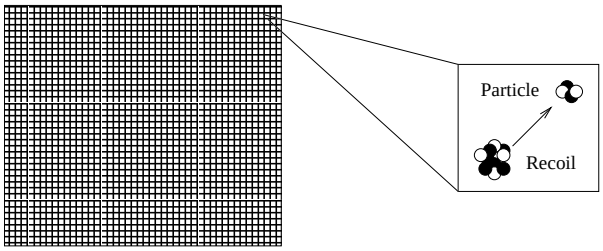

Figure 2.7: Schematic picture of implanted recoil and its corresponding decay in the DSSD at the focal plane.

When studying nuclei very far from stability via fusion-evaporation reactions the reaction channels of interest are normally submerged in the background from the main fusion products, incomplete fusion, fission, Coulomb excitation, etc. The selection sensitivity is therefore very important, otherwise the separation of γ rays that belong to a particular populated channel with low cross section is not possible. In Fig. 2.8 γ-ray spectra from the present work are shown to illustrate the high selectivity that has been achieved. The lower part displays the total γ ray spectrum resulting from the experiment using the reaction ^{54}Fe+^{54}Fe $\rightarrow$^{108}Te*. The upper part displays the prompt γ rays tagged by the α decay of ^{106}Te. Comparing the cross section for population of ^{106}Te, which is estimated to be 25 nb, with the total fusion cross section of the reaction which is about 250 mb, gives a selectivity in order of 10^{-7}. This is probably the highest selectivity which can be achieved for in-beam γ-ray spectroscopy using today's technology.

2.9 Half-Life Measurement

The time information of the recorded data can be used to measure the half lives of nuclear states that decay by emitting α particles or protons. In this work the half lives of the alpha-emitting states in the ^{106}Te and ^{107}Te were measured. This is done by creating histograms of the time differences between the detection of a recoil implantation and its subsequent alpha decay in the same pixel of the DSSDs. These histograms reflect the Poisson distribution of the decay of the implanted recoils. One way of extracting the half life is by fitting a sum of exponential functions to the data points:

$$N = A\exp^{(-\lambda t)} + B\exp^{(-rt)}. \tag{2.4}$$

The half life is calculated from λ, the decay constant, which is a parameter obtained as a result of the fit. The parameter r in equation (2.4) is related to the rate of

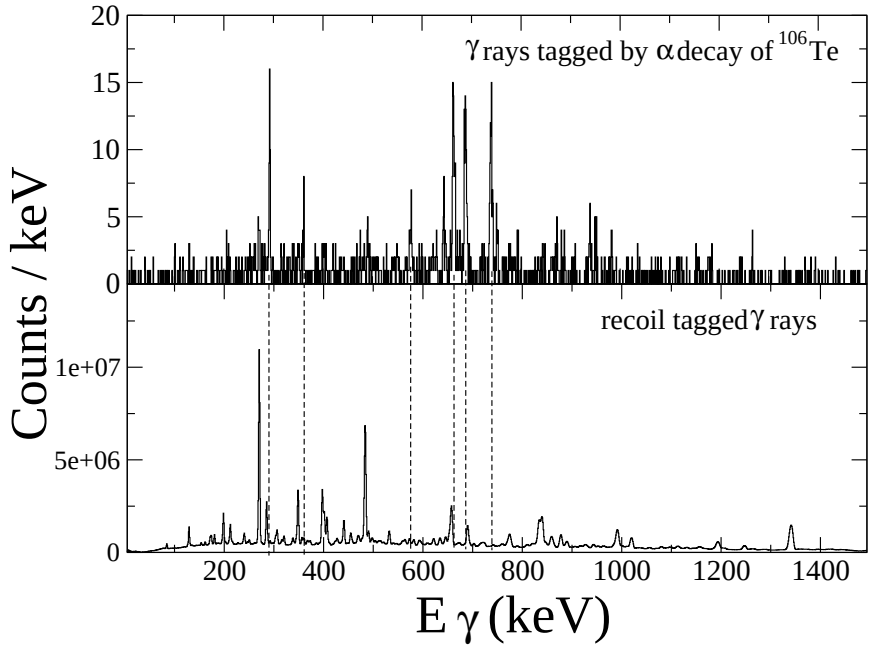

Figure 2.8: In the lower part the total recoil-tagged γ-ray spectrum from the ^{54}Fe+^{54}Fe $\rightarrow^{108}$Te* reaction is shown. The upper panel shows a spectrum of γ rays tagged by ^{106}Te α decay.

random background events and can be estimated from the recoil rate per pixel during the experiment. Another method is the so-called Maximum Likelihood method, which is useful in cases of low statistics and for time spectra with no background contributions [29]. Considering n decays at times $t_1, t_2, ..., t_n \leq T$, the probability of observing a decay between time t and $t + dt$ is given by

$$P(\lambda, t) = \frac{e^{-\lambda t}}{\int_0^T e^{-\lambda t}} = \lambda e^{-\lambda t} dt (1 - e^{-\lambda T})^{-1} \tag{2.5}$$

So, the probability of observing the decays at time $t_1, t_2, ..., t_n$ is

$$P(\lambda, t_1, ..., t_n) = \prod_{i=1}^{n} P(\lambda, t_i) \tag{2.6}$$

The decay constant can be obtained by finding which value of λ has a maximum probability by the following procedure:

$$\frac{\partial log P(\lambda, t_1, ..., t_n)}{\partial \lambda} = 0 \tag{2.7}$$

which gives

$$\lambda = \frac{1}{n}\sum_{i=1}^{n}(t_i) + \frac{T}{e^{\lambda T} - 1}, \tag{2.8}$$

where λ is the decay constant. It is obtained by iteration until convergence of equation (2.8) is achieved. The upper and lower uncertainty limits can be approximated as [30]

$$\begin{aligned} \lambda_u &\approx \frac{\lambda}{1 - \frac{1}{\sqrt{n}}} \\ \lambda_l &\approx \frac{\lambda}{1 + \frac{1}{\sqrt{n}}}. \end{aligned} \tag{2.9}$$

Then the half-life can been obtained from

$$t_{1/2} = \frac{ln2}{\lambda}. \tag{2.10}$$

2.10 Angular Distribution Measurement

The angular distributions of the γ rays emitted from the reaction products can provide some information about the multipolarity of the transitions under study. However, in the case of limited statistics accurate results can be difficult to obtain. In the simplest case, assuming there is no mixing of different multipolarities and that a reasonable spin alignment of the reaction products is present, the angular distribution can to lowest order be written as

$$P(\theta) = 1 + \alpha_2 A_2 P_2(cos\theta) + \alpha_4 A_4 P_4(cos\theta). \tag{2.11}$$

The values of the parameters A_2, A_4, and of the attenuation coefficient α_4 are tabulated in [31]. The attenuation coefficient α_2 can be extracted from a transition with known multipolarity. Using an array of detectors, it is possible to study how the intensity of a particular transition is distributed over different angles. Comparing this experimental result with the theoretically calculated distribution obtained from equation (2.11) allows us to identify the multipolarity of the transition.

A rough approximation which can be used in case of low statistics is to measure and compare the intensity of the transitions in the backward or forward detectors with those at ninety degrees. The result can be formulated as follows:

$$\frac{I_{\gamma(\text{backward or forward})}}{I_\gamma(90^\circ)} \approx \begin{cases} 0.5 & \text{dipole} \\ 1.2 & \text{quadrupole} \end{cases} \tag{2.12}$$

If there is enough statistics the DCO ratio (R_{DCO}) can be measured. It is defined as

$$\frac{I_{\gamma 1}(\text{backward or forward})\text{gated by}I_{\gamma 2}(90^\circ)}{I_{\gamma 1}(90^\circ)\text{gated by}I_{\gamma 2}(\text{backward or forward})} \approx \begin{cases} 0.5 & \text{dipole} \\ 1.2 & \text{quadrupole} \end{cases} \tag{2.13}$$

Knowing the multipolarities of the transitions and the spin of a band head one can assign spins to the excited states in the level scheme.

Chapter 3

Summary of Papers

This thesis describes experiments based on the recoil-decay tagging technique and were performed at the Accelerator Laboratory of the University of Jyväskylä, Finland. The extremely neutron deficient nuclei ^{107}Te and ^{106}Te were produced in fusion-evaporation reactions induced by ^{52}Cr and ^{54}Fe ion beams from the K130 cyclotron. Prompt γ rays produced in the reactions were detected by the Jurogam γ-ray spectrometer. The γ rays belonging to the reaction channel of interest were selected based on the recoil identification provided by the RITU gas-filled recoil separator and the GREAT focal plane spectrometer.

3.1 Paper I

In paper I γ-ray transitions in ^{107}Te have been identified for the first time. The reaction ^{58}Ni(^{52}Cr,3n)^{107}Te* was used to populate the ^{107}Te nuclei in excited states. The production cross section was estimated to be 1μb. The first excited state at 90 keV with the spin and parity $7/2^{+}$, tentatively of $g_{7/2}$ character, is proposed. This assignment is supported by the observation by Schardt *et al.* of two α-decay lines at 3480(30) keV and 3580(30) keV associated with the decay of ^{111}Xe [32]. We suggest that a 721 keV line deexcites a tentative $9/2^{+}$ state to the $5/2^{+}$ ground state, whereas a 631 keV line deexcites the same state to a first excited $7/2^{+}$ state at 90 keV. The low excitation energy of the first excited state is interesting in relation to astrophysical models of the rp process, which is predicted to end at the nucleus ^{107}Te due to (γ, α) reactions. By comparing the excitation energy of this state with those of the corresponding states in the heavier Te isotopes and in the Sn isotopic chain we found different trends as N→Z. This points to increased influence from n-p correlations near N=Z.

3.2 Paper II

In paper II, γ-ray transitions in ^{106}Te have been identified for the first time. The reaction ^{54}Fe(^{54}Fe,2n)^{106}Te* was used with an estimated production cross section of 25 nb, a new limit for in-beam γ-ray spectroscopy. A ground-state band, tentatively extending up to $I^{\pi} = 10^{+}$, is proposed. The systematics of low-lying yrast states in the Te isotopes is discussed within the context of vibrational excitations and residual nucleon-nucleon interactions. Evidence for enhanced collectivity near N=Z due to neutron-proton correlation is discussed.

Acknowledgments

First, I would like to thank my supervisor, Bo Cederwall, for giving me the opportunity to further study in nuclear physics and for his support. Many thanks to Karin Lagergren who has helped me establishing my work and has been encouraging me in all steps. I thank Arne Johnson for helping me in various ways. Thanks to Torbjörn Bäck who with his impressive way of explaining, helped me to understand many new concepts. Thanks to Lars-Olov Norlin, Ramon Wyss, Jan Blomqvist, Roberto Liotta and Andras Kerek who helped me finding the answer to many questions. I would like to thank Karin Andgren, Mikael Sandzelius, Anton Khaplanov, Larissa Milechina, Daniel Karlgren, Shufang Ban, Ela Ganioğlu and the reactor physics group for their friendship and helpfulness. I thank Adrin Cavani for his helps, Irina Zartova for her friendship, and Suzan Langlet for being nice to me. Last and most of all I thank my family for their incredible amount of love and support.

Bibliography

[1] M. Goeppert, Phys. Rev. 75, 1969, 1949.

[2] K. L. G.Heyde, *The Nuclear Shell Model*, Springer-Verlag 1994.

[3] R. F. Casten, *Nuclear structure from a single perspective,* Oxford science publication 1990.

[4] B. Hadinia *et al.*,, Phys. Rev. C72, 41303(R), 2005.

[5] D. L. Hill and J.A.Wheeler, Phys. Rev. 89, 1102, 1953.

[6] T. Bäck, *Spectroscopy of Neutron Deficient Nuclei in the* $A \approx 90$ *and* $A \approx 170$ *Mass Regions*, (2002).

[7] C. F. von Weizäcker, Z. Phys. 96, 341,1935.

[8] H.A.Bethe and R.F.Bacher, Rev. Mod. Phys.8,82,1936.

[9] S. G. Nilsson and I. Ragnarsson, *Shape and Shells in Nuclear Structure.* Cambridge University Press, 1995.

[10] V. M. Strutinsky, Nucl. Phys. A95, 420, 1967.

[11] S. G. Nilsson, Nucl. Phys. A122, 1, 1968.

[12] N. Bohr and F. Kalckar, Danske Vidensk. Selsk. Mat.-Fys. Meddr. (Skr.) 14,10, 1937.

[13] A. Bohr, Mat. Fys. Medd. Dan Vid.Selsk, 26, No.14, 1952.

[14] A. Bohr and B. Mottelson, Mat. Fys. Medd. Dan Vid.Selsk, 27, No.16, 1952.

[15] W. Satuła and R. Wyss *Phys. Scripta*, T 56, 159 (1995).

[16] H. Schatz *et al.*, Phy. Rev. Lett. 86, No.16,2001.

[17] E. S. Paul *et al.*, Phys. Rev. C51, 78, 1995.

[18] R.S. Simon *et al.*, Z .Phys. A325, 197, 1986.

[19] M. Leino *et al.*, Nucl. Instr. Meth. B99, 653, 1995.

[20] M. Leino, Nucl. Instr. Meth. B126, 320 1997.

[21] http://www.phys.jyu.fi/

[22] P. T. Greenless *Identification of Excited States and Evidence for Octupole Deformation in* ^{226}U, (1999).

[23] C. W. Beausang *et al.*, Nucl. Instr. Meth. A313, 37, 1992.

[24] A. Ghiorso*et al.*, NIM A, 269:192, 1988.

[25] A. P. Leppänen *Alpha-decay and decay-tagging studies of heavy elements using the RITU separator*, (2005).

[26] I. H. Lazarus *et al.*, IEEE Trans. Nucl. Sci48, 567, 2001.

[27] P. Rahkila, To be submitted to Nucl.Instr.Meth.A

[28] H.-Q. Jin, *priv. comm.*

[29] E. Segre, *Nuclei and Particles, An Introduction to Nuclear and Subnuclear Pysics*. W.A.Benjamin, New York, 1964.

[30] K. H. Schmidt *et al.*, Z. Phys.A,316:19,1984.

[31] T. Yamazaki, Nucl.Data. 3, 1 ,1967.

[32] D. Schardt *et al.*, Nucl. Phys. A368, 153 (1981).